Title

Molecular investigation of gas adsorption, separation, and transport on carbon nanoscrolls: A combined grand canonical Monte Carlo and molecular dynamics study

Authors

Sha, Haoyan
Zhang, Shenli
Faller, Roland

Publication Date

2018-06-01

DOI

10.1016/j.carbon.2018.02.078

Peer reviewed

Molecular Investigation of Gas Adsorption, Separation, and Transport on Carbon Nanoscrolls: A Combined Grand Canonical Monte Carlo and Molecular Dynamics Study

Haoyan Sha[1], Shenli Zhang[2], Roland Faller[11]

[1] Department of Chemical Engineering, University of California, Davis, Davis, CA, 95616

[2] Department of Materials Science and Engineering, University of California, Davis, Davis, CA, 95616

ABSTRACT

Carbon nanoscrolls (CNSs), with controllable interlayer distances, have been systematically studied with respect to noble gas adsorption, separation, and transport properties. Grand canonical Monte Carlo simulations were performed on pure noble gases and noble gas mixtures interacting with CNSs at different temperatures. There is separation of gases across a series of CNS interlayer distances at different pressures. The optimal interlayer distance for each noble gas was determined. Selective adsorption was characterized for noble gas mixtures, and the corresponding selectivity was explored. A molecular sieving effect was observed for a certain interlayer gap range, in which the energetically unfavorable smaller gas atoms were better stored in the CNS. In addition, molecular dynamics simulations were conducted to understand the transport properties of noble gases in carbon nanoscrolls in both

1 Corresponding author. E-mail: rfaller@ucdavis.edu

the cross-sectional and axial directions of the CNS. Gas molecules are found to be captured most strongly when the CNS has the optimal interlayer distance for adsorption.

Keywords: carbon nanoscrolls, gas adsorption, grand canonical Monte Carlo (GCMC), molecular dynamics

1. Introduction

Layered carbon nanomaterials with hexagonally packed carbon surface structures have attracted extensive attention in the past few decades due to their excellent thermodynamic, mechanical, and electrical properties. This enables next generation functional materials for various applications [1-8]. Particularly, the large specific surface area and lightweight nature make them great novel gas storage/separation materials and transport media. A number of different morphologies of such carbon nanomaterials have been discovered, including carbon nanotubes, graphene, carbon nanohorns, etc. [5, 6]

Carbon nanoscrolls (CNSs) are a new member in this group of materials. They can be considered as rolled-up graphene sheets [9-13]. They are distinct from other 2-D carbon nanomaterials as they have a potentially controllable inter-carbon layer distance. As reported experimentally and computationally the interlayer space can be controlled by alkali metal doping [14, 15]. This makes CNSs a very promising material for selective gas adsorption and separation.

For the study of gas adsorption and transport in layered nanoporous materials, molecular simulations have been extensively applied, as they provide atomic information that is hard to obtain experimentally. Most simulation effort has been directed to nanotube structures made of carbon and boron nitride. Several reviews have summarized the discoveries of structural, thermal, mechanical and other properties [16-21]. Gas adsorption and transport properties of these materials are also widely investigated [22-35].

A few molecular simulation studies on nanoscrolls have been reported. Braga et al. applied molecular dynamics (MD) to study the structural stability of carbon nanoscrolls [13]. They found that the overlap area of the rolled sheets and the inner circle diameter are critical for stabilizing CNSs. Similarly boron nitride nanoscrolls were studied by the same group [36]. The corresponding equilibrium structures were predicted. Xia et al. studied by MD the formation of CNSs from graphene initiated by a carbon nanotube in the center [37]. A similar strategy to prepare CNSs was reported by Chu et al. with a silicon nanowire as seed [38]. Mpourmpakis et al. demonstrated the effect of CNS interlayer spacing on hydrogen storage by combined quantum chemistry and GCMC [14]. Braga et al. simulated hydrogen adsorption by MD[15]. Daff et al. investigated the separation of CO_2 by CNSs with GCMC [39]. Peng et al. studied the adsorption of methane and carbon dioxide [40].

To our knowledge, the adsorption of noble gases, which are important adsorbates in both industry and academia, on carbon nanoscrolls has not yet been studied. Also generally, the understanding of the selective adsorption and separation of gas mixtures in CNSs is still underdeveloped. No transport properties of gases and gas mixtures in CNSs have been

reported. Here, a systematic study has been performed on CNSs interacting with different noble gases for a range of CNS interlayer distances. Specifically, grand canonical Monte Carlo (GCMC) simulations were used to understand the adsorption of pure noble gases on CNSs and the selective adsorption and separation of noble gas mixtures at different temperatures. The optimal CNS interlayer distance for each case was determined. Inverted selective adsorption was observed in a small CNS interlayer spacing window for some noble gas mixtures. The mixture composition effect on noble gas selective adsorption was also investigated. In addition, the noble gas transport in CNS was simulated by MD. The mean squared displacement (MSD) was analyzed.

2. Simulation Model & Method

Carbon nanoscroll simulation models were developed from a graphene sheet of 50x10 nm by rolling along the long side and keeping the CNS length at 10 nm, as shown in Figure 1. The CNS cross-section can be expressed by the formula:

$$r(\theta) = r_0 + t\theta \quad (1)$$

where r_0 is the inner circle radius, t is the interlayer distance, θ is the polar angle, and r is the polar coordinate representing the distance of the sheet from the center.

Figure 1. *Visualization of the Carbon nanoscroll model*

The inner radius r_0 was set to 10.0 Å, which yields the energetically favorite curvature [13]. Interlayer distances t from 6.0 to 10.0 Å in 0.5 Å steps were tested for gas adsorption/separation and transport characterizations. The carbon – carbon bond length was fixed at 1.42 Å. The CNS was kept rigid through all the simulations. Periodic boundary conditions were applied. We ensured that CNSs did not cross-talk with mirror configurations.

Classical Lennard – Jones 12-6 potentials were selected for the Van der Waals interactions with a cutoff distance of 20 Å:

$$\phi_{ij} = 4\,\varepsilon_{ij}\left[\left(\sigma_{ij}/r\right)^{12} - \left(\sigma_{ij}/r\right)^{6}\right] \quad (2)$$

where σ_{ij} is the interaction length and ε_{ij} is the potential energy well depth. The corresponding parameters are listed in Table 1 [41, 42]. The carbon – gas interaction parameters are approximated by Lorentz – Berthelot mixing rules:

$$\varepsilon_{ij}=\sqrt{\varepsilon_{ii}\varepsilon_{jj}} \qquad \sigma_{ij}=(\sigma_{ii}+\sigma_{jj})/2 \quad (3)$$

No electrostatic interactions were taken into account.

Table 1. *Lennard – Jones 12-6 potential parameters of carbon and noble gases*

Element	ε/k_B (K)	σ (Å)
C	28.2	3.4
Ar	120	3.4
Kr	171	3.6
Xe	221	4.1

Grand canonical Monte Carlo (GCMC) simulations with fixed chemical potential, volume, and temperature were performed with the MCCCS Towhee code [43] for gas adsorption and separation. The chemical potentials of the gas phase were derived from separate isothermal–isobaric simulations using the Widom insertion method [44]. We used insertion/deletion and translation moves with probabilities of 0.25/0.25 and 0.5, respectively. For gas mixtures, an interatomic exchange move was introduced to accelerate equilibration (insertion/deletion – 0.2/0.2, translation – 0.4, exchange – 0.2). All GCMC simulations were performed for 2×10^7

steps, where the first 10^7 MC steps were used to equilibrate the system and the second 10^7 were for data collection.

MD simulations in the canonical ensemble (NVT) were performed with the LAMMPS code [45] for gas transport. The initial configurations were taken from the equilibrated GCMC simulations. The velocity-Verlet algorithm was used for time integration [46], and the Nosé – Hoover thermostat for temperature control [47, 48]. All MD simulations were run for 6 ns with a time step of 1 fs. Despite the short times the MSDs (below) show that the systems are well equilibrated. The MD force field was the same as in GCMC for consistency.

3. Result & Discussion

3.1 Grand Canonical Monte Carlo simulations

Pure noble gases, Ar, Kr, and Xe, adsorbed on the selected CNSs at 300 K were studied with GCMC simulations. The adsorption data was collected at different pressures (10^4 - 10^6 Pa), and the corresponding data are shown in Fig. 2. All adsorption isotherms are expressed in absolute terms, which counts all gas molecules in the system with no further bias. It can be found that by opening the CNS interlayer spacing from 6 Å to 10 Å, the adsorption of each gas first increases and then drops to different extents. That is because with a narrow gap, CNS expresses strong repulsion towards the gas atoms, which inhibits the gas to enter the interlayer space. When it opens up, the repulsion weakens and eventually turns into adsorption until it reaches the optimal distance. At further opening, the attractive interaction decreases. Comparing across the three noble gases, the optimal CNS interlayer distance is dependent on

the gas size and interaction strength with carbon. In terms of adsorption capacity at the corresponding optimum CNS configuration, Xenon with the largest atomic mass and strongest interaction with carbon was the most adsorbed. Kr is second, and Ar is the weakest adsorbed. At different pressures the adsorption behaviors express different trends. At low pressure, the enhancement due to proper interlayer distance significantly increases the adsorption, especially for Xe. At higher pressures, the interaction is not adsorption, it is more storage. The opening up of the CNS interlayer gap allows more noble gas atoms to be packed into the space. The optimal CNS interlayer distances for noble gas adsorption are summarized in Table 2, they weakly grow with gas size.

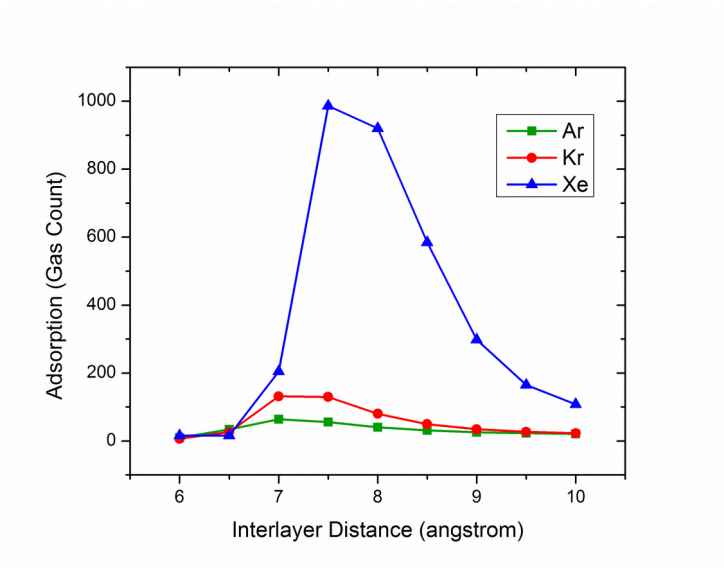

(a)

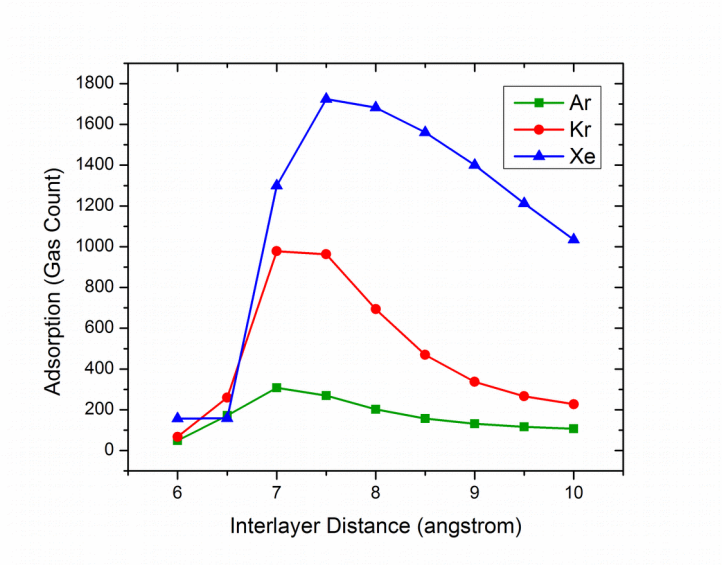

(b)

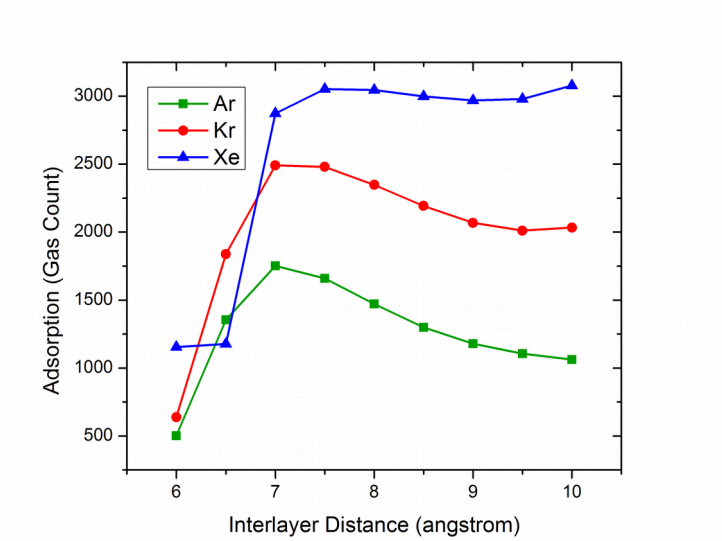

(c)

Figure 2. *Adsorption dependence of pure noble gases as a function of interlayer distance on and in CNSs at 300 K and (a) 10^4 Pa, (b) 10^5 Pa, (c) 10^6 Pa*

Table 2. *Optimal CNS interlayer distance for noble gas adsorption. Errors are 0.25-0.5 Å in distance. For Xe at the highest pressure we cannot clearly determine an optimum.* For Kr where the two highest values are very close we chose the average interlayer distance as maximum.

Noble Gas	Pressure (Pa)	Interlayer Distance

		(Å)
Ar	10^4	7
	10^5	7
	10^6	7
Kr	10^4	7.25
	10^5	7.25
	10^6	7.25
Xe	10^4	7.5
	10^5	7.5
	10^6	(7.5-10)

To characterize the CNS interlayer distance effect on noble gas adsorption, potential energy distribution was studied by scanning an individual noble gas atom in the lateral direction and cross the center of mass of the CNS, as shown in Figure 3. It is found that at interlayer space of 6.0 Å the potential energy wells only exist on the most outside surface and the inner circle surface of the CNS. All interlayer space shows strong repulsion on the noble gas atom. Comparing the noble gases, Xe, which has the strongest interaction with carbon, presents the deepest potential well, while Ar with the lowest atomic mass among these three elements shows the weakest adsorption potential. When the gap opens up to 8.0 Å, the interlayer space is large enough to accommodate all three noble gases and presents very strong adsorption wells (much deeper than the wells on the CNS outside surface and inner circle). This stems from the confinement effect of the carbon layers. The net potential on the gas atom is very attractive inside the interlayer gaps. Then by further raising the interlayer distance to 10.0 Å, the interlayer potential wells are broadened, but the depths become shallower. Note that the potential energy profiles on the CNS outside surface and inner circle stay almost the same in all cases. This analysis explains the different of noble gas adsorption on CNS with different interlayer distances.

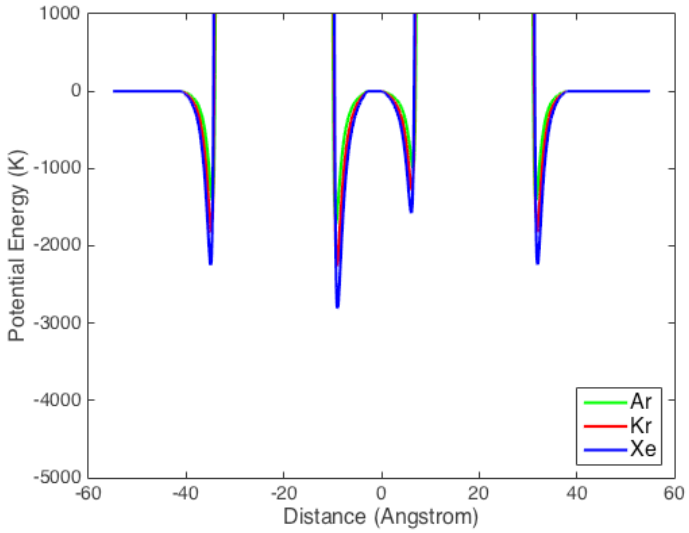
1000
0
-1000
-2000
-3000
-4000
-5000
Potential Energy (K)
-60
-40
-20
0
20
40
60
Distance (Angstrom)
Ar
Kr
Xe

(a)

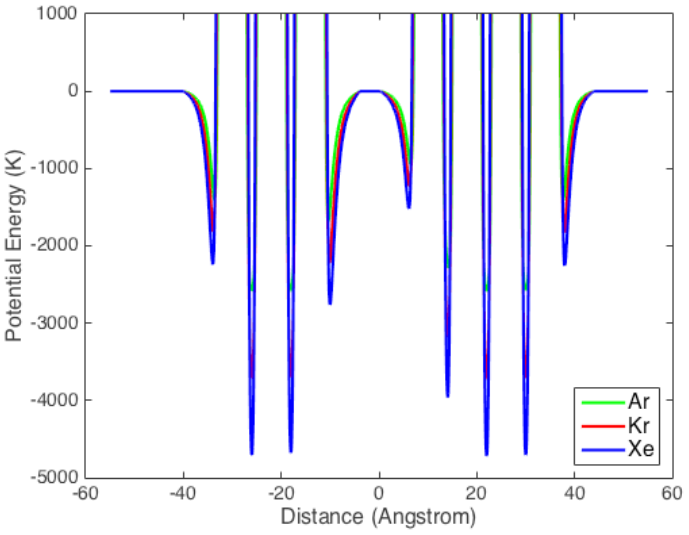
1000
0
-1000
-2000
-3000
-4000
-5000
Potential Energy (K)
-60
-40
-20
0
20
40
60
Distance (Angstrom)
Ar
Kr
Xe

(b)

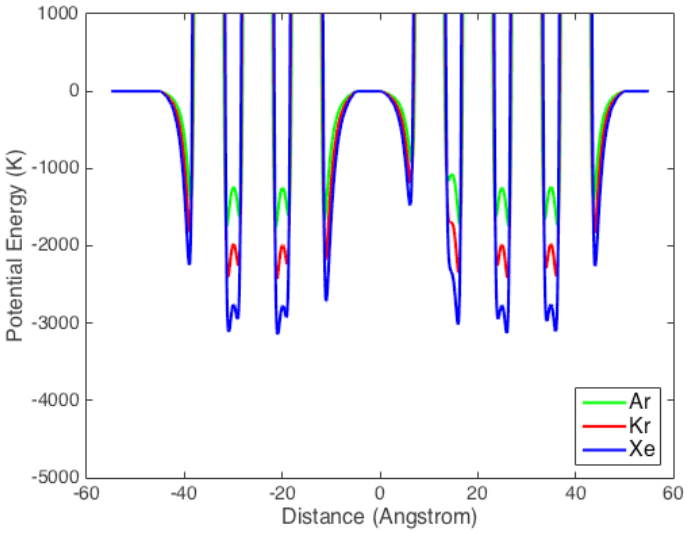

(c)

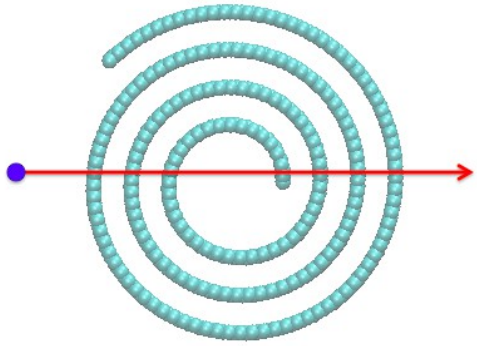

(d)

Figure 3. *Potential energy distribution of noble gases interacting with CNSs with interlayer distances of (a) 6.0 Å, (b) 8.0 Å, (c) 10.0 Å, (d) schema: green - top view of 8.0 Å CNS, blue – noble gas atom, red – scanning direction*

Furthermore, the isosteric heat of adsorption of pure noble gases on CNSs was investigated using the following expression:

$$q = RT - \frac{\langle EN \rangle - \langle E \rangle \langle N \rangle}{Var(N)}$$

where E is the energy, N is the number of adsorbed gas molecules, T is the temperature, and R is the gas constant. $Var(N)$ represents the variance in particle numbers. The heat of adsorption data was collected from Ar adsorption on CNSs at 300 K for different pressures (Fig. 4). The trends correspond well with the adsorption data and further explain the adsorption in CNSs with varying interlayer distances, where gas uptake is determined by the competition between energy and entropy/packing effects.

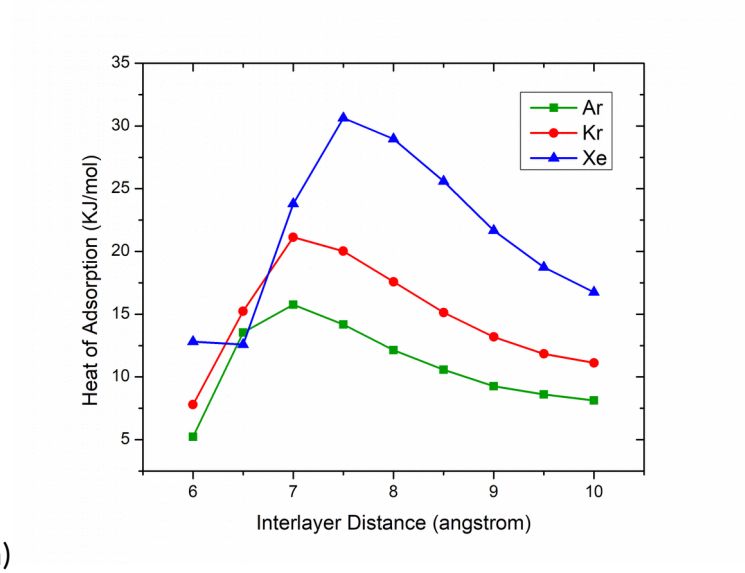

(a)

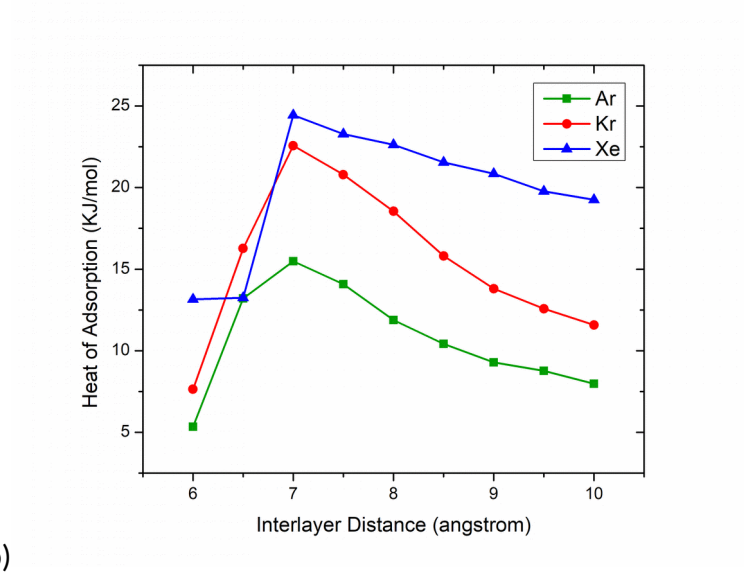

(b)

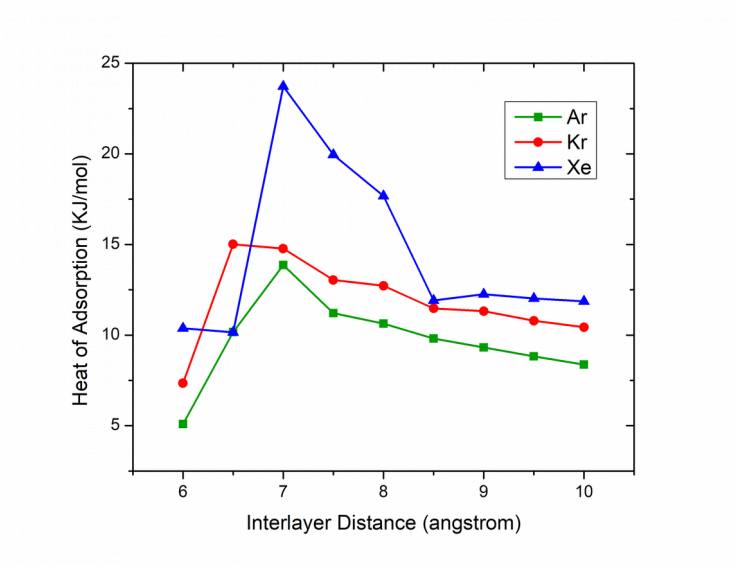

(c)

Figure 4. Heat of adsorption of Ar as a function of interlayer distance on and in CNSs at 300 K and (a) 10^4 Pa, (b) 10^5 Pa, (c) 10^6 Pa

In addition, noble gas adsorption on CNS is also studied at 100 K, as shown in Figure 5. Comparing to the 300 K adsorption set, GCMC simulations were performed on CNSs with different interlayer spacing, but the selected pressure range is lower as noble gases have much lower condensation pressures at 100 K. From the figures, we see that at 100 Pa with broadening the interlayer spacing, the adsorptions of Kr and Xe keep rising, while Ar increases

at the beginning and becomes stable around 8.5 Å, then drops greatly. This is mainly due to the change in inter-carbon layer confinement strength. At the given pressure, for Ar with relatively weaker potential strength with CNS, when a strong potential well forms, Ar atoms are adsorbed the most. When the gap becomes larger, the confinement effect is weakened and it cannot attract so many gas atoms as the interaction distances to sheets on either side increase. On the other hand, for Kr and Xe with strong interatomic interaction with carbons, the enlarged space helps accommodate more gas atoms. This trend can be observed in Fig. 5b and 5c. As the pressure goes lower, Kr, which is largely adsorbed at large CNS interlayer gap, starts to drop as Ar, while the optimal adsorption gap becomes narrower and narrower.

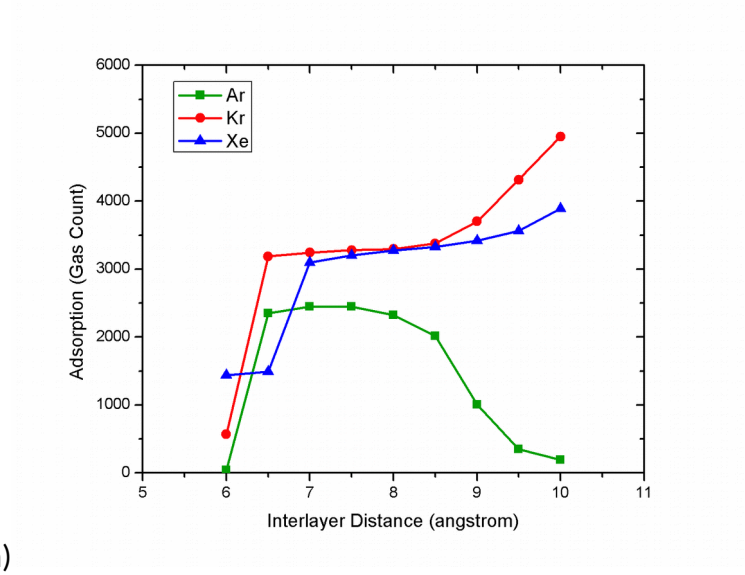

(a)

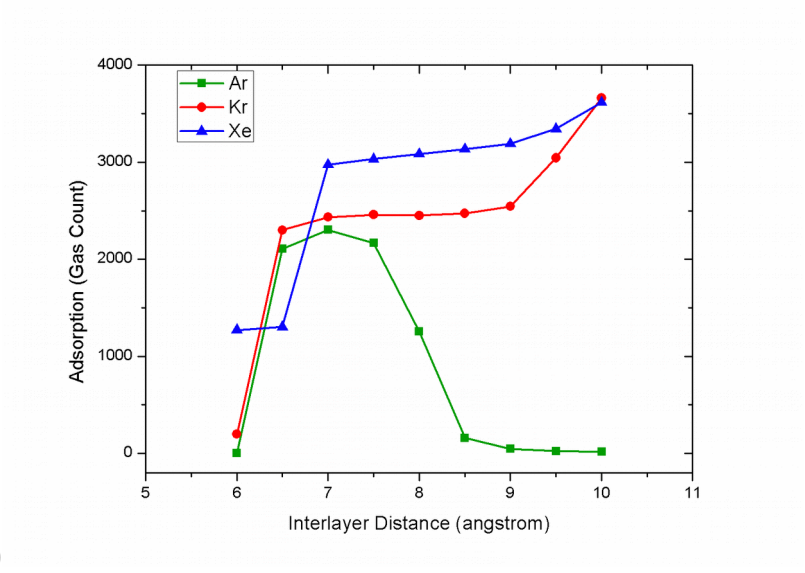

(b)

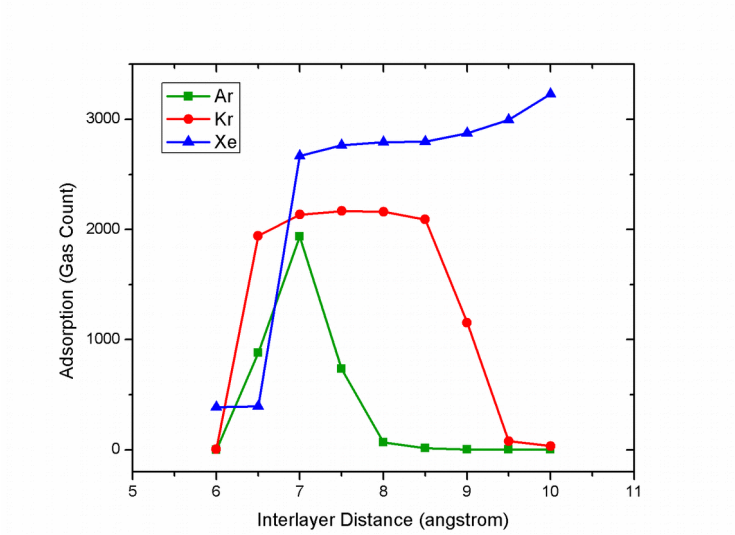

(c)

Figure 5. *Adsorption dependence of pure noble gases as a function of interlayer distance on and in CNSs at 100 K and (a) 100 Pa, (b) 10 Pa, (c) 1 Pa*

Inspired by the observation of slightly different optimal CNS interlayer distances for the pure noble gases, the study was extended to gas mixtures regarding selective adsorption and separation. Binary noble gas mixtures with equal partial pressure loadings were simulated at

300 K. Figure 6 shows the data of Kr – Xe at various pressures. A similar trend as in the pure gas cases was observed at low pressure. The adsorption of the larger and heavier Xe is stronger than that of Kr, especially at the CNS interlayer spacing around 8 Å. At high pressure, however, the adsorption selectivity is inverted at a specific CNS interlayer spacing window, in which the energetically unfavorable smaller and lighter gas was better adsorbed over the larger atoms. This inversion of adsorption is caused by the balance of adsorption and packing. At high pressure, the system can pack more molecules in the finite space.

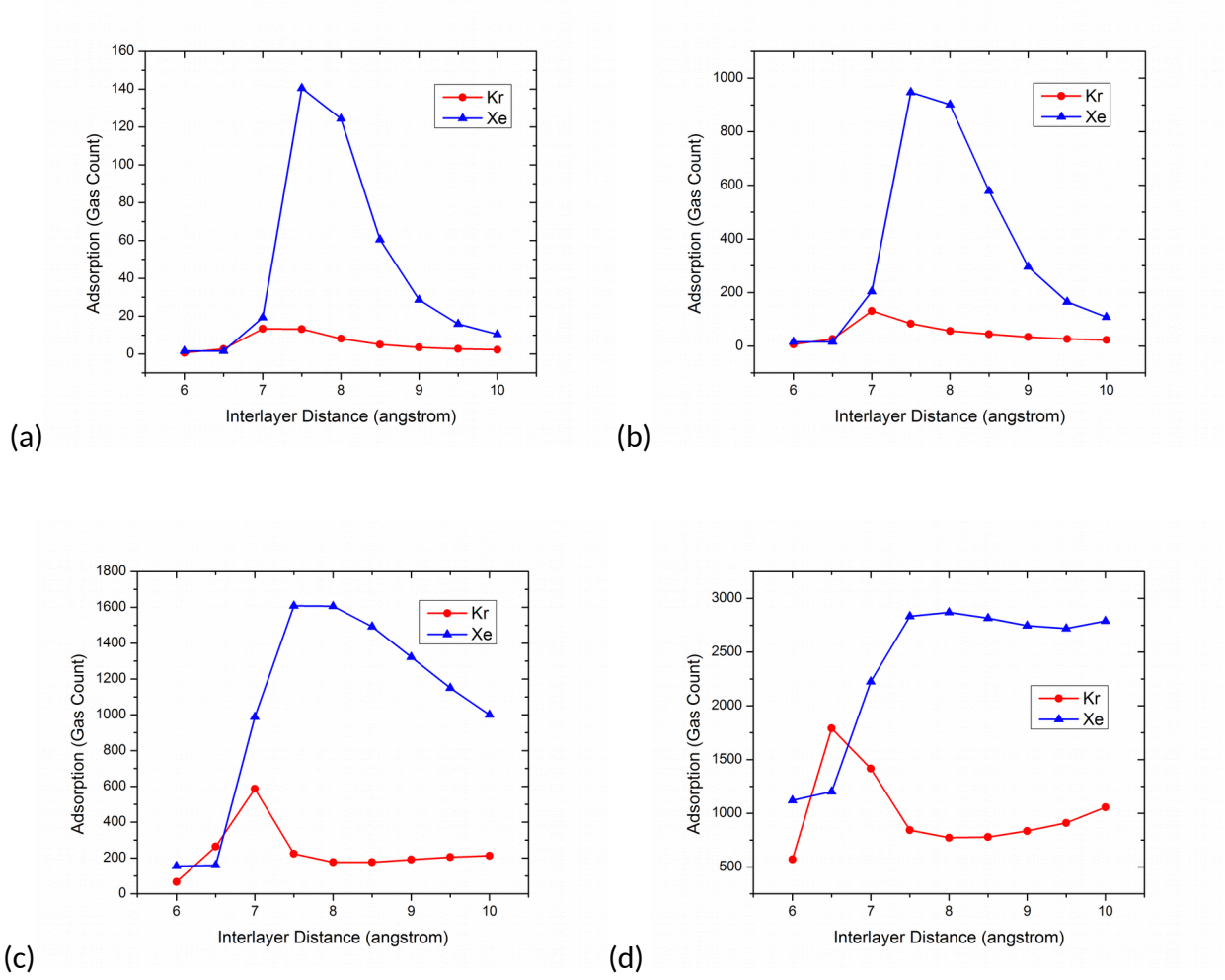

Figure 6. *Adsorption dependence of equimolar Kr – Xe mixtures as a function of interlayer distance at 300 K and element partial pressure of (a) 10^3 Pa, (b) 10^4 Pa, (c) 10^5 Pa, (d) 10^6 Pa. Note that this means the total pressure is double these values.*

Figure 7 shows the adsorption dependence of the binary gas mixture Ar – Kr. The data shows a similar adsorption selectivity trend as Kr – Xe. Here, the inverted adsorption for Ar – Kr is found from 6.0 Å to 6.5 Å, which is smaller than for Kr – Xe. The distinction is mainly due to the atomic size difference between the two components. It is also found that the optimal interlayer distances for Ar and Kr are close in the low-pressure regime, but become more separated at higher pressure. Note, that the optimum for Ar with presence of Kr shifts to smaller interlayer distances compared to pure Ar.

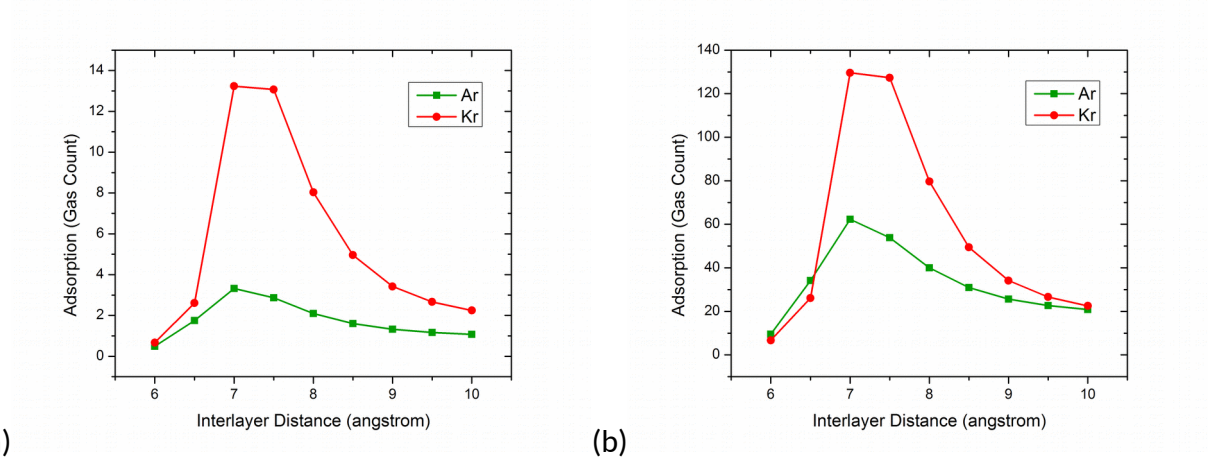

(a) (b)

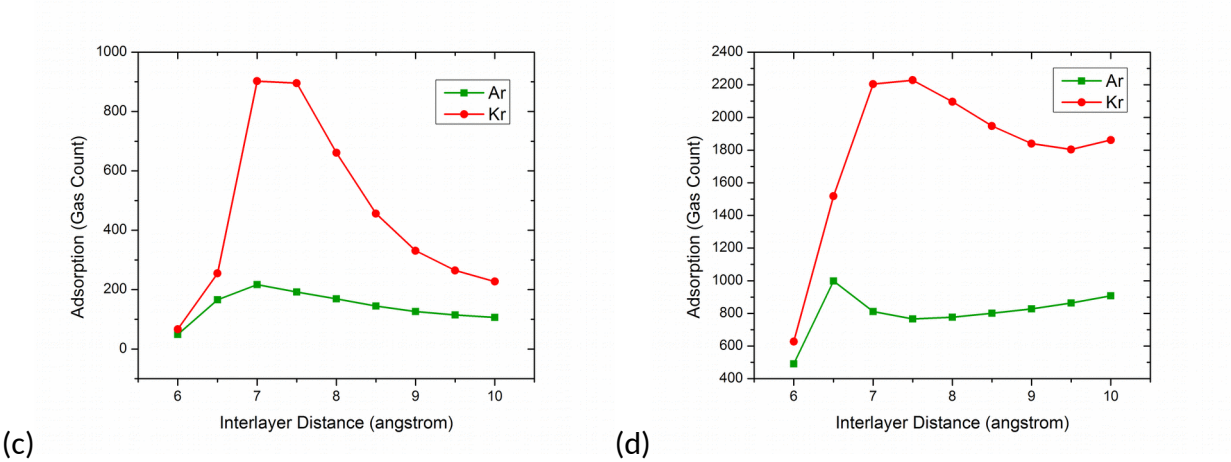

Figure 7. *Adsorption dependence of equimolar Ar – Kr mixtures as a function of interlayer distance at 300 K and element partial pressure of (a) 10^3 Pa,(b) 10^4 Pa, (c) 10^5 Pa, (d) 10^6 Pa*

The adsorption data at different CNS interlayer distances provides information on the net adsorption and separation of a specific component in the mixtures. To further characterize the detailed distribution of each gas component in CNS, the radial distribution function (RDF) was employed to analyze the equilibrated GCMC simulation configurations of noble gas mixtures in CNSs. The RDF plots of Kr-Xe and the corresponding simulation snapshots are shown in Fig. 8. For the Kr-Xe mixture, at short CNS interlayer distance (less than 6.0 Å), the adsorption of both components is on the outside surfaces and the innermost cylinder space of the CNS. Xe with stronger interaction with carbon is more adsorbed compared to Kr. When the gap is increased to 6.5 Å, Kr becomes moderately adsorbed to the interlayer space in the CNS, while Xe is still too large to fit in the gap. The selectivity of Kr over Xe inverted. By further increasing the gap, xenon starts to enter the CNS and moves the selectivity towards Xe.

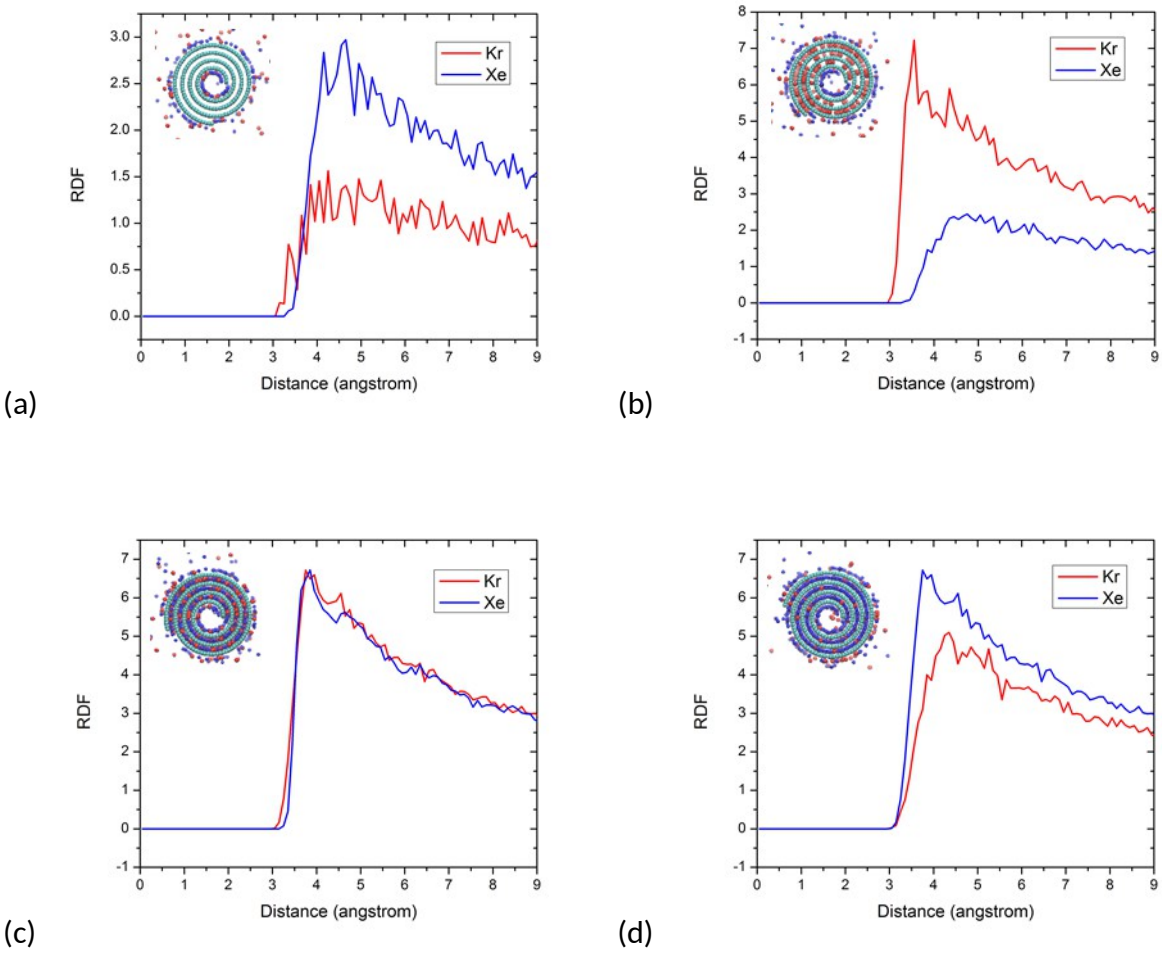

Figure 8. *Radial distribution functions of Kr and Xe with carbon at 300 K and 10^5 Pa in the Kr – Xe gas mixture adsorbed on CNS with interlayer distance at (a) 6.0 Å, (b) 6.5 Å, (c) 7.0 Å, (d) 7.5 Å. Insets are the corresponding GCMC simulation snapshots*

Also, the adsorption selectivity of Kr/Xe on carbon nanoscrolls was calculated and compared with the results collected with carbon nanotubes (CNT) at 300 K and different pressures, as shown in Figure 9. Here, (10, 10) armchair type CNT, which is the most abundant type observed in experiments [49, 50], was used for this study. It is observed that CNT prefers to adsorb more Xe over Kr at the selected pressures. For CNSs, the selectivity of Kr/Xe highly

depends on the interlayer distance. In specific, at relatively small CNS interlayer distance ranges, the selectivity of Kr/Xe on CNS is above 1, which means Kr atoms are preferred adsorbates. By increasing the gap, the selectivity is inversed and the selectivity of Xe over Kr is slight higher on CNSs than CNTs.

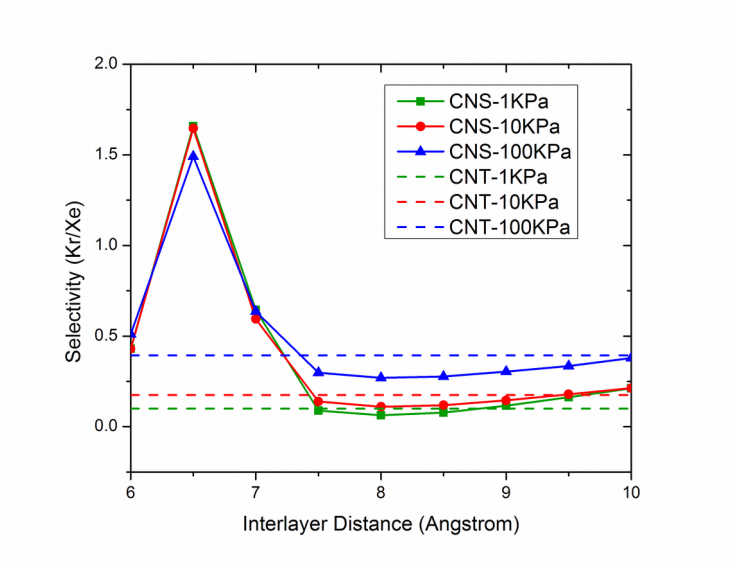

Figure 9. Comparison of CNS and CNT on Kr-Xe mixture selective adsorption at 300 K. Selectivity is expressed as the ratio of the adsorption of Kr/Xe.

Additionally, the mixture composition effect on the selective adsorption was explored with Kr – Xe mixture at 300 K on CNS with different interlayer distances. Xe composition was changed from 10% to 90%, while keeping the total gas loading at 10^5 Pa. The adsorption data is presented in Figure 10. It can be found that xenon adsorption increases with the higher loading composition in all selected CNSs. By increasing the CNS interlayer distance, besides the change of gas adsorption amount, the selectivity of Xe/Kr also changes. At 6.0 Å the adsorption mainly takes place on CNS' outside surface and inner circle. The adsorption curve is very linear to Xe composition. When the interlayer distance rises to 8.0 Å, the selectivity of Xe over Kr is

improved, which is contributed to the confinement effect between the carbon layers. By further enlarge the gap to 10.0 Å, the adsorption curve becomes close to linear again.

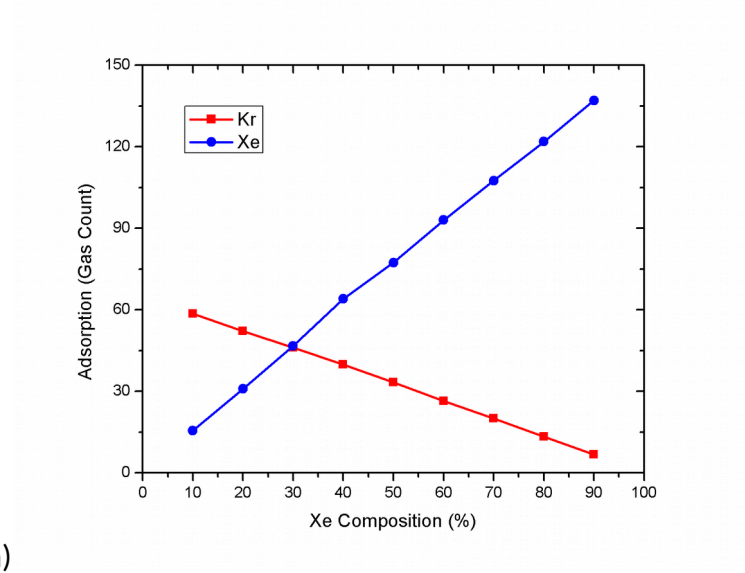

(a)

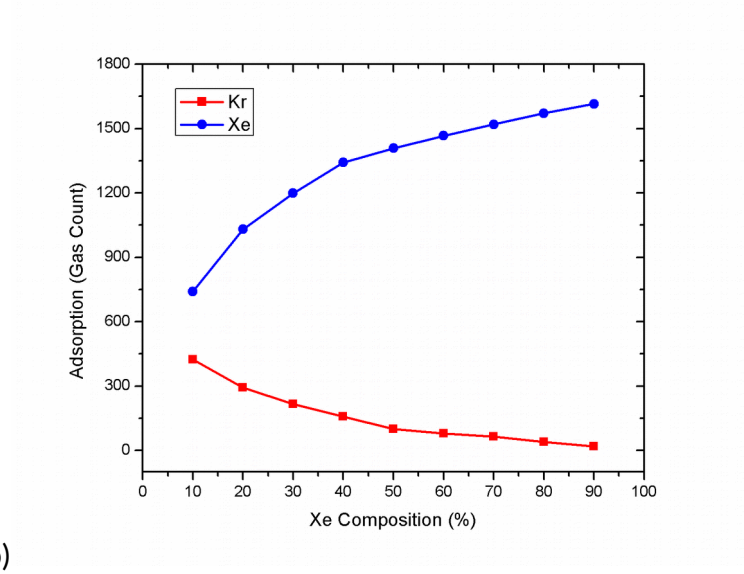

(b)

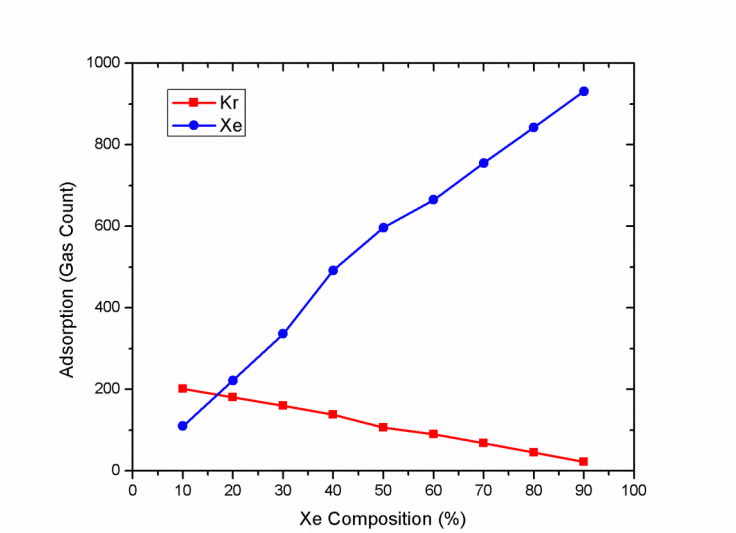

(c)

Figure 10. *Adsorption dependence of Kr – Xe mixtures as a function of mixture composition at 300 K on CNS with interlayer distances of (a) 6.0 Å, (b) 8.0 Å, (c) 10.0 Å*

3.2 Molecular Dynamics simulations

In addition to the study of equilibrium adsorption and separation, we also investigated the transport of pure noble gases and noble gas mixtures in CNS systems by MD, which is widely used to study transport properties [51-53]. Mean squared displacements (MSD) characterize the overall gas transport as well as their radial and axial components.

Figure 11 shows the overall MSD of Kr transport in CNSs for a series of interlayer distances at 300 K and 1 bar. At the very narrow spacing of 6.0 Å, the MSD is very large representing fast transport. In this case, no Kr atom is inside the CNS interlayer. All gas atoms move freely. By broadening the gap, the MSD quickly drops as gas atoms are confined in the interlayer volume. The mobility reaches the lowest value when the inter-CNS distance is optimal for Kr adsorption (7.5 Å). Increasing the gap further, the MSD increases again. The adsorption

spacing of CNS allowing most gas molecules to enter also immobilizes the adsorbed gas most in the interlayer space, since it is the energetically favorite configuration.

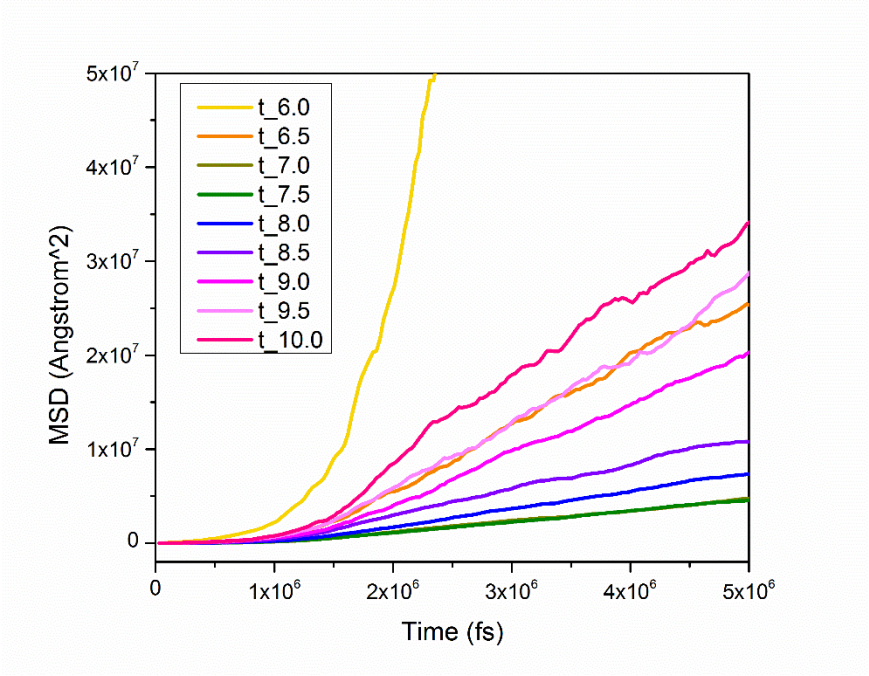

Figure 11. *Mean squared displacement of Krypton adsorbed in CNS with different interlayer spacing at 300 K and 1 bar*

In addition to the overall MSD of Krypton, MSD components in different directions are plotted in Figure 12. The range of CNS interlayer spacing covers the range from no gas inside to the optimal adsorption cases. We find that the major contributions come from the axial direction where there is no steric hindrance.

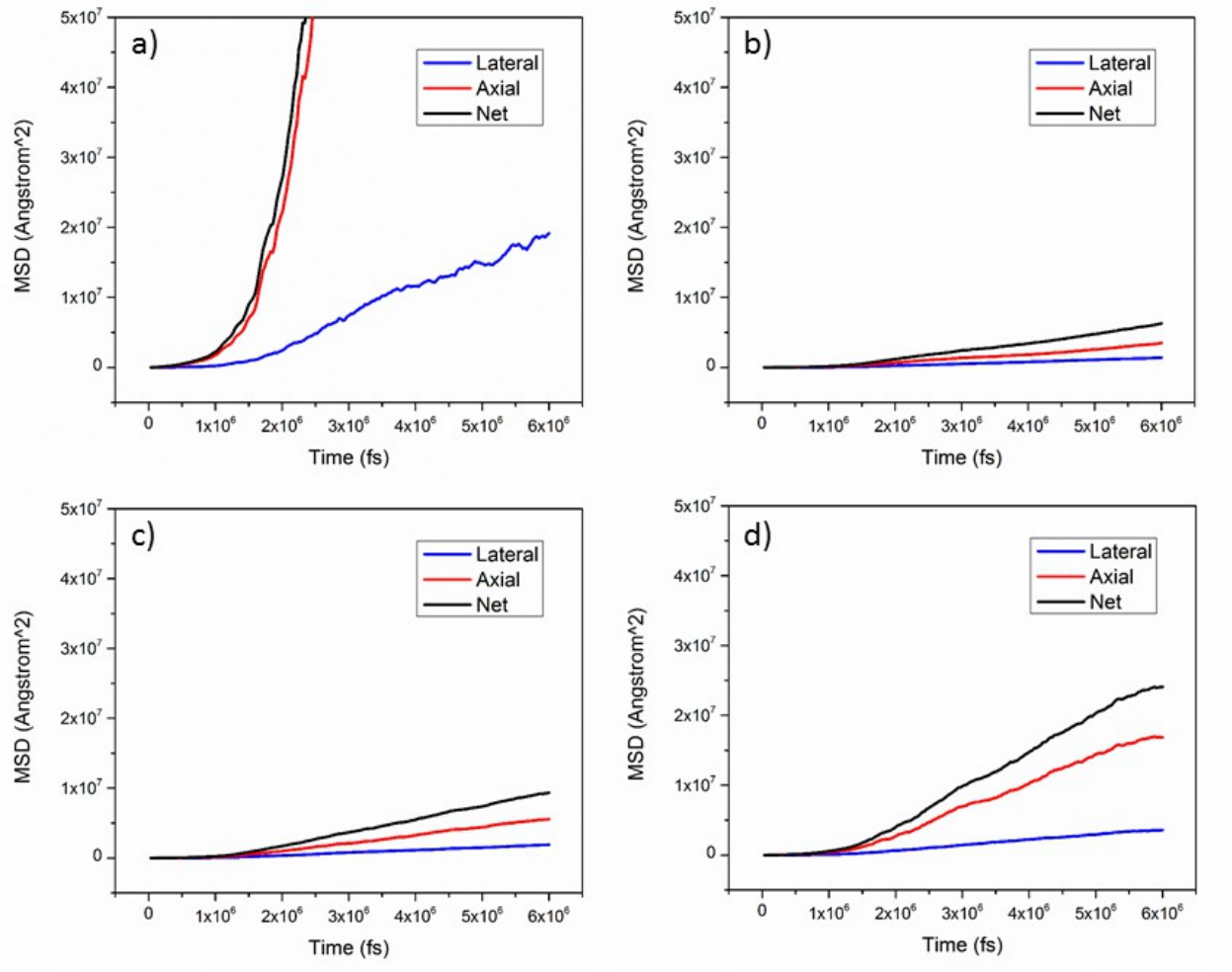

Figure 12. Mean squared displacement of Krypton adsorbed in CNS in different directions with different interlayer spacing of (a) 6.0 Å, (b) 7.0 Å, (c) 8.0 Å, (d) 9.0 Å

4. Conclusion

We systematically studied noble gas adsorption, separation, and transport in carbon nanoscrolls with different interlayer distances (from 6.0 Å to 10.0 Å). Grand canonical Monte Carlo simulations were applied to understand noble gas adsorption and storage in CNS at different pressures and temperatures. Selective adsorption was investigated on noble gas mixtures. The optimal CNS interlayer distances for pure and mixed noble gases were

determined. Radial distribution function and simulation snapshots are used to supplement the adsorption data and suggest detailed distribution of each gas component in the CNS system. At a given temperature and pressure, the selectivity is strongly dependent on the CNS interlayer distance. The selectivity depends non-monotonically on this distance and on pressure which is different than for carbon nanotubes where the selectivity is mainly pressure dependent and depends monotonically on pressure [22]. In addition, the mixture composition effect on selective adsorption was investigated with Kr-Xe mixture by tuning Xe composition from 10% to 90%, while keeping the total gas loading the same. Selective adsorption is observed in all cases but with distinct selectivity.

The transport properties of CNS were studied with molecular dynamics in the canonical ensemble. The mean square displacement data of Krypton shows that the confinement of CNS applied on gas molecules first becomes stronger with increasing interlayer distance and drops after reaching a maximum. The gas molecules are best stabilized in the CNS interlayer space at the specific optimal interlayer distance.

ACKNOWLEDGEMENTS

This research was supported by the U.S. Department of Energy, Office of Nuclear Energy, under Grant No. DE-NE0000704.

References

[1] S. Iijima, Carbon nanotubes: past, present, and future, Physica B: Condensed Matter 323(1–4) (2002) 1-5.
[2] R. Hirlekar, M. Yamagar, H. Garse, M. Vij, V. Kadam, Carbon nanotubes and its applications: a review, Asian Journal of Pharmaceutical and Clinical Research 2(4) (2009) 17-27.
[3] R.E. Morris, P.S. Wheatley, Gas Storage in Nanoporous Materials, Angewandte Chemie International Edition 47(27) (2008) 4966-4981.
[4] H. Dai, Carbon Nanotubes: Synthesis, Integration, and Properties, Accounts of Chemical Research 35(12) (2002) 1035-1044.
[5] M.J. Allen, V.C. Tung, R.B. Kaner, Honeycomb Carbon: A Review of Graphene, Chemical Reviews 110(1) (2010) 132-145.
[6] E.T. Thostenson, Z. Ren, T.-W. Chou, Advances in the science and technology of carbon nanotubes and their composites: a review, Composites science and technology 61(13) (2001) 1899-1912.
[7] M.I. Katsnelson, Graphene: carbon in two dimensions, Materials today 10(1) (2007) 20-27.
[8] A.A. Balandin, Thermal properties of graphene and nanostructured carbon materials, 10 (2011) 569.
[9] X. Shi, N.M. Pugno, H. Gao, Mechanics of carbon nanoscrolls: a review, Acta Mechanica Solida Sinica 23(6) (2010) 484-497.
[10] M.M. Zaeri, S. Ziaei-Rad, Elastic properties of carbon nanoscrolls, Rsc Advances 4(44) (2014) 22995-23001.
[11] L.M. Viculis, J.J. Mack, R.B. Kaner, A chemical route to carbon nanoscrolls, Science 299(5611) (2003) 1361-1361.
[12] E. Perim, L.D. Machado, D.S. Galvao, A Brief Review on Syntheses, Structures, and Applications of Nanoscrolls, Frontiers in Materials 1 (2014) 31.
[13] S.F. Braga, V.R. Coluci, S.B. Legoas, R. Giro, D.S. Galvão, R.H. Baughman, Structure and Dynamics of Carbon Nanoscrolls, Nano Letters 4(5) (2004) 881-884.
[14] G. Mpourmpakis, E. Tylianakis, G.E. Froudakis, Carbon nanoscrolls: a promising material for hydrogen storage, Nano letters 7(7) (2007) 1893-1897.
[15] S. Braga, V. Coluci, R. Baughman, D. Galvao, Hydrogen storage in carbon nanoscrolls: An atomistic molecular dynamics study, Chemical physics letters 441(1) (2007) 78-82.
[16] S. Agnihotri, J.P.B. Mota, M. Rostam-Abadi, M.J. Rood, Structural Characterization of Single-Walled Carbon Nanotube Bundles by Experiment and Molecular Simulation, Langmuir 21(3) (2005) 896-904.
[17] Y. Lin, J.W. Connell, Advances in 2D boron nitride nanostructures: nanosheets, nanoribbons, nanomeshes, and hybrids with graphene, Nanoscale 4(22) (2012) 6908-6939.
[18] R.S. Ruoff, D.C. Lorents, Mechanical and thermal properties of carbon nanotubes, carbon 33(7) (1995) 925-930.
[19] N.G. Chopra, R. Luyken, K. Cherrey, V.H. Crespi, Boron nitride nanotubes, Science 269(5226) (1995) 966.
[20] D. Golberg, Y. Bando, C.C. Tang, C.Y. Zhi, Boron Nitride Nanotubes, Advanced Materials 19(18) (2007) 2413-2432.
[21] D. Golberg, Y. Bando, Y. Huang, T. Terao, M. Mitome, C. Tang, C. Zhi, Boron Nitride Nanotubes and Nanosheets, ACS Nano 4(6) (2010) 2979-2993.
[22] H. Sha, R. Faller, Molecular simulation of adsorption and separation of pure noble gases and noble gas mixtures on single wall carbon nanotubes, Computational Materials Science 114 (2016) 160-166.

[23] S. Zhang, H. Sha, E. Yu, M.P. Page, R. Castro, P. Stroeve, J. Tringe, R. Faller, Computational and Experimental Studies on Novel Materials for Fission Gas Capture, in: J.H. Jackson, D. Paraventi, M. Wright (Eds.), Proceedings of the 18th International Conference on Environmental Degradation of Materials in Nuclear Power Systems – Water Reactors: Volume 1, Springer International Publishing, Cham, 2018, pp. 1039-1050.
[24] N. Dawass, M.L. D'Lima, I.G. Economou, M. Castier, Phase Equilibrium with External Fields: Application to Confined Fluids, Journal of Chemical & Engineering Data 61(8) (2016) 2873-2885.
[25] K. Wu, Z. Chen, X. Li, X. Dong, Methane storage in nanoporous material at supercritical temperature over a wide range of pressures, Scientific Reports 6 (2016) 33461.
[26] P. Billemont, B. Coasne, G. De Weireld, Adsorption of Carbon Dioxide, Methane, and Their Mixtures in Porous Carbons: Effect of Surface Chemistry, Water Content, and Pore Disorder, Langmuir 29(10) (2013) 3328-3338.
[27] M. Lasich, D. Ramjugernath, Influence of unlike dispersive interactions on methane adsorption in graphite: a grand canonical Monte Carlo simulation and classical density functional theory study, The European Physical Journal B 88(11) (2015) 313.
[28] H. Sha, R. Faller, A quantum chemistry study of curvature effects on boron nitride nanotubes/nanosheets for gas adsorption, Physical Chemistry Chemical Physics 18(29) (2016) 19944-19949.
[29] X. Li, Y. Jin, Q. Xue, L. Zhu, W. Xing, H. Zheng, Z. Liu, Ultra-high selective capture of CO 2 on one-sided N-doped carbon nanoscrolls, Journal of CO2 Utilization 18 (2017) 275-282.
[30] X. Li, Q. Xue, X. Chang, L. Zhu, H. Zheng, Fluorine-rich carbon nanoscrolls for CO2/CO (C2H2) adsorptive separation, Journal of CO2 Utilization 21(Supplement C) (2017) 429-435.
[31] X. Chang, Q. Xue, D. He, L. Zhu, X. Li, B. Tao, 585 divacancy-defective germanene as a hydrogen separation membrane: A DFT study, International Journal of Hydrogen Energy 42(38) (2017) 24189-24196.
[32] L. Zhu, Q. Xue, X. Li, T. Wu, Y. Jin, W. Xing, C2N: an excellent two-dimensional monolayer membrane for He separation, Journal of Materials Chemistry A 3(42) (2015) 21351-21356.
[33] S. Zhang, M. Perez-Page, K. Guan, E. Yu, J. Tringe, R.H. Castro, R. Faller, P. Stroeve, Response to Extreme Temperatures of Mesoporous Silica MCM-41: Porous Structure Transformation Simulation and Modification of Gas Adsorption Properties, Langmuir 32(44) (2016) 11422-11431.
[34] R. Majidi, Molecular Dynamics Simulation of Noble Gases Adsorption on Carbon Nanotube Bundles, Fullerenes, Nanotubes and Carbon Nanostructures 22(6) (2014) 520-527.
[35] D. Mantzalis, N. Asproulis, D. Drikakis, Enhanced carbon dioxide adsorption through carbon nanoscrolls, Physical Review E 84(6) (2011) 066304.
[36] P. Eric, S.G. Douglas, The structure and dynamics of boron nitride nanoscrolls, Nanotechnology 20(33) (2009) 335702.
[37] D. Xia, Q. Xue, J. Xie, H. Chen, C. Lv, F. Besenbacher, M. Dong, Fabrication of carbon nanoscrolls from monolayer graphene, Small 6(18) (2010).
[38] L. Chu, Q. Xue, T. Zhang, C. Ling, Fabrication of carbon nanoscrolls from monolayer graphene controlled by p-doped silicon nanowires: a md simulation study, The Journal of Physical Chemistry C 115(31) (2011) 15217-15224.
[39] T.D. Daff, S.P. Collins, H. Dureckova, E. Perim, M.S. Skaf, D.S. Galvão, T.K. Woo, Evaluation of carbon nanoscroll materials for post-combustion CO 2 capture, Carbon 101 (2016) 218-225.
[40] X. Peng, J. Zhou, W. Wang, D. Cao, Computer simulation for storage of methane and capture of carbon dioxide in carbon nanoscrolls by expansion of interlayer spacing, Carbon 48(13) (2010) 3760-3768.
[41] G. Stan, M.J. Bojan, S. Curtarolo, S.M. Gatica, M.W. Cole, Uptake of gases in bundles of carbon nanotubes, Physical Review B 62(3) (2000) 2173-2180.

[42] R.O. Watts, I.J. McGee, Liquid State CHemical Physics, Wiley, New York, 1976.
[43] M.G. Martin, MCCCS Towhee: a tool for Monte Carlo molecular simulation, Molecular Simulation 39(14-15) (2013) 1212-1222.
[44] B. Widom, Some Topics in the Theory of Fluids, J. Chem. Phys. 39(11) (1963) 2808-2812.
[45] S. Plimpton, Fast Parallel Algorithms for Short-Range Molecular Dynamics, Journal of Computational Physics 117(1) (1995) 1-19.
[46] W.C. Swope, H.C. Andersen, P.H. Berens, K.R. Wilson, A computer simulation method for the calculation of equilibrium constants for the formation of physical clusters of molecules: Application to small water clusters, The Journal of Chemical Physics 76(1) (1982) 637-649.
[47] S. Nose, A unified formulation of the constant temperature molecular-dynamics methods, J. Chem. Phys. 81(1) (1984) 511-519.
[48] W.G. Hoover, Canonical dynamics - Equilibrium phase-space distributions, Phys. Rev. A 31(3) (1985) 1695-1697.
[49] A. Kuznetsova, J.T. Yates, J. Liu, R.E. Smalley, Physical adsorption of xenon in open single walled carbon nanotubes: Observation of a quasi-one-dimensional confined Xe phase, Journal of Chemical Physics 112(21) (2000) 9590-9598.
[50] J. Liu, A.G. Rinzler, H. Dai, J.H. Hafner, R.K. Bradley, P.J. Boul, A. Lu, T. Iverson, K. Shelimov, C.B. Huffman, F. Rodriguez-Macias, Y.-S. Shon, T.R. Lee, D.T. Colbert, R.E. Smalley, Fullerene Pipes, Science 280(5367) (1998) 1253-1256.
[51] H. Sha, R. Faller, G. Tetiker, P. Woytowitz, Molecular simulation study of aluminum–noble gas interfacial thermal accommodation coefficients, AIChE Journal 64(1) (2018) 338-345.
[52] M. Foroutan, A. Taghavi Nasrabadi, Adsorption and separation of binary mixtures of noble gases on single-walled carbon nanotube bundles, Physica E: Low-dimensional Systems and Nanostructures 43(4) (2011) 851-856.
[53] A.I. Skoulidas, D.M. Ackerman, J.K. Johnson, D.S. Sholl, Rapid Transport of Gases in Carbon Nanotubes, Physical Review Letters 89(18) (2002) 185901.